ACS APPLIED MATERIALS & INTERFACES

www.acsami.org Research Article

Plant Transpiration-Inspired Biomass-Based Device with Underwater Oleophobicity for Efficient General-Purpose Solar-Driven Oily Wastewater Purification

Zhenglong Xu, Yifan Yang, Wei Yao, Chuming Ye, Haohui Qiao, Jianfeng Shen,* and Mingxin Ye*

Cite This: *ACS Appl. Mater. Interfaces* 2023, 15, 48336−48345 Read Online

ABSTRACT: The remediation of wastewater containing oily pollutants is imperative to mitigate the serious threats posed to the safety of fresh water, human well-being, and the environment. Current membrane separation technologies are severely restricted by their limitations for separating various types of oily pollutants with low sustainability. Herein, by imitating the plant transpiration in nature, we designed a solar-driven device composed of natural biomass sugar cane stem, chitosan/carboxymethyl cellulose, and graphite powders to separate versatile oily pollutants from the wastewater. Owing to its superior solar absorption capacity, microchannels for water transportation, and underwater oleophobicity, the resultant evaporator not only exhibited an excellent evaporation rate of 1.41 kg m^{-2} h^{-1} but also demonstrated an admirable purification efficiency of 99.9% for oily wastewater. Moreover, the device can maintain a stable evaporation rate and the original structure even in oily wastewater containing strong acid, alkali, or hypersaline components. Therefore, this work provides an effective approach to producing clean water from versatile wastewater.

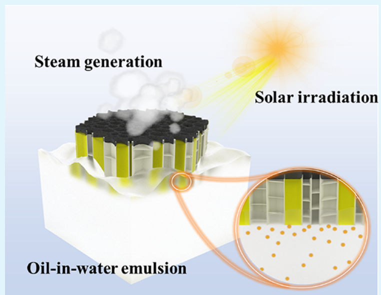

KEYWORDS: *wastewater purification, oily pollutants, solar-driven, plants transpiration, underwater oleophobicity*

1. INTRODUCTION

At present, oily wastewater from domestic activities and industrial emissions have severely threatened drinking water safety, human health, and ecological environment.[1−4] It is thus essential to advance effective and green technologies to remediate oily wastewater. Conventional approaches for the treatment of the oil/water mixture include centrifugation separation, gravity separation,[5] physical adsorption,[6] and chemical treatment,[7] which all have obvious disadvantages of environmental pollution, high capital, and inefficient separation. Currently, membrane separation has received considerable attention due to its relatively simple operational processes.[8−12] For instance, the MXene membrane,[13] covalent organic framework membrane,[14] polytetrafluoroethylene membrane,[15] polycaprolactone-mixed supramolecular framework fiber membrane,[16] cobalt phosphide/stainless steel mesh membrane,[17] and fish gelatin membrane[18] have been prepared to efficiently handle oily wastewater. However, it is complicated to realize the purification of various types of oily wastewater with only one membrane because there are not only oil droplets but also salt ions, organic and acids, or alkaline pollutants in oily wastewater.[2,19,20] Therefore, the efficient purification of oil/water mixtures to obtain fresh water is still an urgent issue that must be addressed.

Recently, as an effective alternative, a solar steam evaporator has been investigated for seawater desalination or wastewater purification. The solar steam generator has emerged as a promising solution to facilitate freshwater production from wastewater or seawater by harnessing solar energy.[21−26] According to the reported literature, inorganic materials, such as semiconductors[27] and metallic nanoparticles,[28,29] and organic materials, such as carbon-based materials[30,31] and polymers materials,[32] have been developed for solar steam evaporation. However, the widespread adoption of this emerging technology is restricted owing to its expensive raw materials and complicated fabrication processes. Furthermore, although solar-driven evaporators can efficiently deal with seawater and brine, the presence of substances like oils, dyes, and organic compounds can clog the microscale channels of solar-thermal devices, leading to diminished evaporation efficiency and potential device damage.[33,34] Inspired by the plant transpiration process, the exodermis of the plant roots serves as a selective barrier against the harmful elements in soil but allows for water infiltration, whereas the vascular bundles inside provide abundant channels for water transportation,[35] and the plant leaves absorb sunlight and vapor escapes through stomata on their surfaces. In this study, the chitosan/carboxymethylcellulose (CS/CMC) gel of the evaporator

Received: August 21, 2023
Accepted: September 21, 2023
Published: October 4, 2023

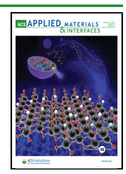

https://doi.org/10.1021/acsami.3c12333
ACS Appl. Mater. Interfaces 2023, 15, 48336−48345

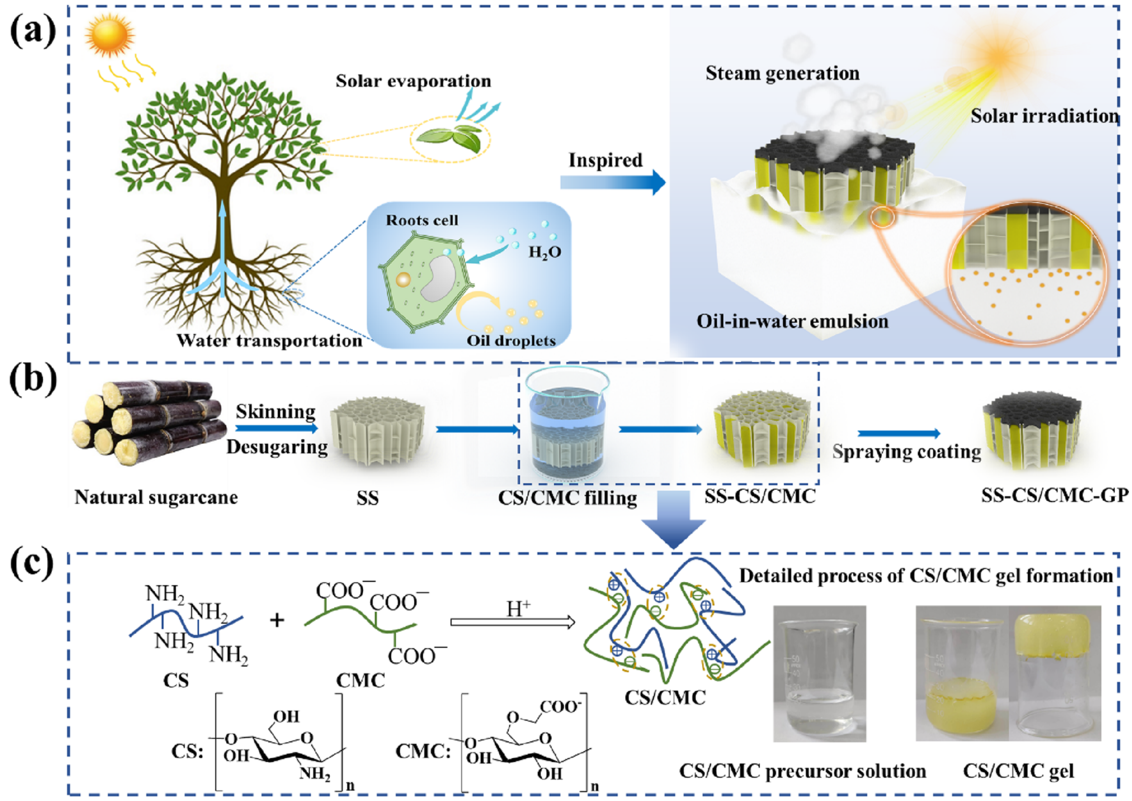

Figure 1. (a) Tree-inspired solar-driven device for purification of oily wastewater. (b) The fabrication process of the solar-driven device. (c) Detailed process of the CS/CMC gelation. The insets are digital images of the CS/CMC precursor solution and CS/CMC gel.

acted as an obstruction to deter the oil droplets while enabling water transport to the upper surface of the evaporator for solar-driven evaporation. CS/CMC plays a significant role in oil resistance. As far as we know, solar-driven technologies are commonly used for water evaporation and seawater desalination, whereas the purification of oil-in-water emulsions in this way has been rarely investigated, especially for the emulsified oily seawater.

Herein, we propose a novel strategy to design a sustainable, low-cost, and multifunctional solar-driven device. We select the desugaring stem of sugar cane (SS) modified by CS/CMC hydrogel fillings and decorated with graphite powders (GPs) on the top surface to prepare the oily wastewater purification system (SS-CS/CMC-GP). The well-distributed microchannels are fairly favorable for the water transportation of the solar-driven evaporator.[36] In addition, owing to its superior hydrophilicity and underwater oleophobicity, the solar-driven device displays a high purification efficiency of 99.9% for an oil-in-water emulsion. Moreover, benefiting from the excellent desalination property and acid-alkali resistance, the device demonstrates a great value in purifying oily seawater and acidic/alkaline oily water to generate freshwater. Furthermore, the evaporator exhibits outstanding long-term durability and an excellent photothermal conversion of 93.3%. All of these promising features indicate that the well-designed SS-CS/CMC-GP solar-powered evaporator is achievable for handling oily wastewater, oily seawater, and domestic sewage. This device demonstrates a significant potential for addressing water scarcity in arid and underdeveloped regions by efficiently extracting clean water from household wastewater. Furthermore, the scalability of the evaporator by increasing its quantity presents promising practical applications, particularly in water-scarce island regions, where solar energy can be utilized to obtain freshwater from seawater.

2. RESULTS AND DISCUSSION

2.1. Fabrication and Schematic of the SS-CS/CMC-GP.

In nature, transpiration is a fundamental physiological process of plants that has been extensively investigated.[37,38] As shown in Figure 1a, under solar illumination, tree leaves harness sunlight and convert it into thermal energy, which is concentrated on the surface of leaves. This concentrated heat energy facilitates the evaporation of liquid water, allowing it to be released into the atmosphere through the leaves. Concurrently, tree roots take up water from the soil and transport it to the leaves through the negative pressure system. This process is facilitated by the capillary force of wood channels, which creates a continuous flow of water from the bottom to the top of the tree.[39] Inspired by the transpiration process of a tree, a bilayer structured solar-driven device composed of SS-CS/CMC that acts as a water transportation layer and GPs as the solar absorption layer was designed to achieve the efficient separation of oily wastewater. GPs are known as superior photothermal conversion materials,[40] whereas SS is an outstanding water-absorbing material with a rapid water transport performance. Furthermore, the CS/CMC gel introduced into the microchannels can be likened to a hydrophilic filter film, which effectively prevents insoluble oil from passing through the bottom of the film. Because of the excellent underwater oleophobicity of SS-CS/CMC, the evaporator is expected to handle different kinds of oily wastewater under solar illumination. During the purification process, water can be transported to the top surface of the device from the bulk wastewater along the microchannels

https://doi.org/10.1021/acsami.3c12333
ACS Appl. Mater. Interfaces 2023, 15, 48336−48345

an9kkhW_Ercy7Dm3ZL_9Cf3qfKAc485ysgAAALcwgbQGCSqGSIb3DQEHBqCBpjCBowIBADCBnQYJKoZIhvcNAQcBMB4GCWCGSAFlAwQBLjARBAzm7zGoWZ1ZdGieEI0CARCAcMhSzno434I5hk-8koOL4zmJP8QErXsA36w-KfiZhodN6N_igUKoaKIQno62c8NOCbvevlcN_LHDVj7CsFmh31g26-Sws

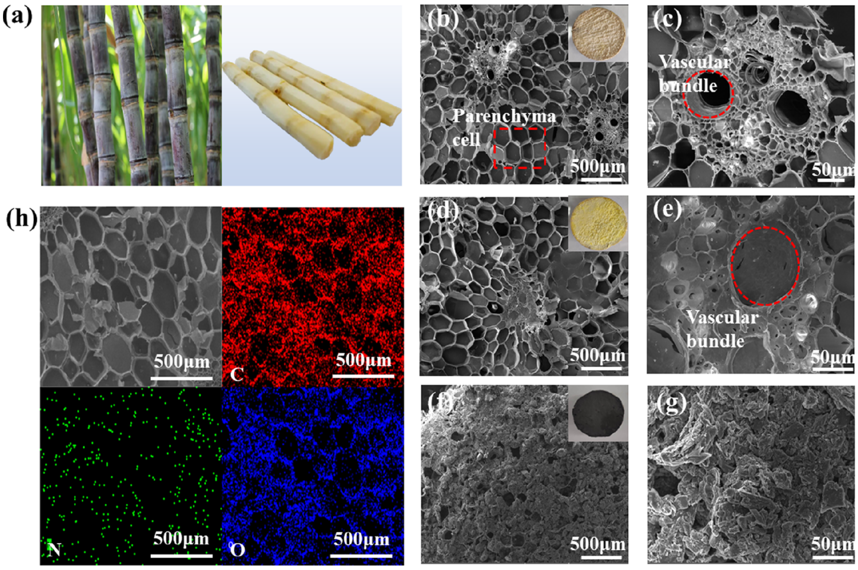

Figure 2. (a) Photograph of sugar cane fruits. Cross-section SEM images of (b, c) SS, (d, e) SS-CS/CMC, and (f, g) SS-CS/CMC-GP, respectively. The insets are optical photos of the corresponding specimens. (h) EDS mapping images of the SS.

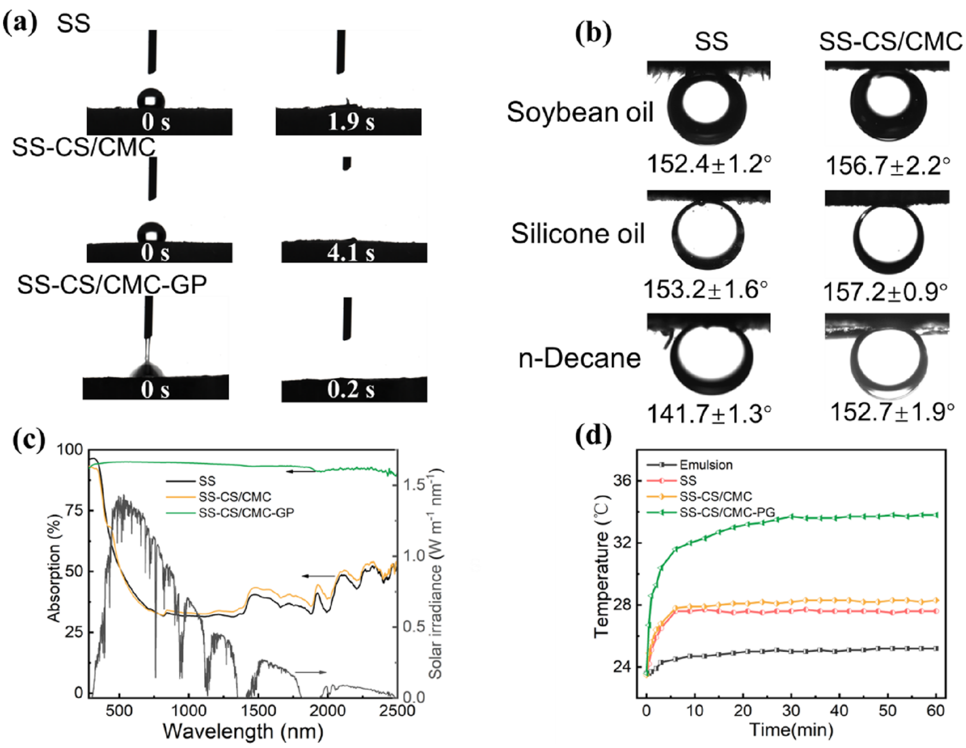

Figure 3. (a) WCAs of SS, SS-CS/CMC, and SS-CS/CMC-GP devices. (b) OCAs of SS and SS-CS/CMC for various oils. (c) UV−vis-NIR light absorption spectra of SS, SS-CS/CMC, and SS-CS/CMC-GP. (d) The temperature changes of SS, SS-CS/CMC, and SS-CS/CMC-GP over time under 1 sun irradiation.

under capillary forces; meanwhile, oil droplets are limited in the bulk wastewater. Under solar illumination, the liquid water is converted to vaporous water, leaving behind solely the pollutants. Subsequently, the vaporous water was condensed on a collector to obtain clean water, thereby successfully realizing the purification of oily wastewater.

The fabrication of the SS-CS/CMC-GP solar-driven evaporator is schematically shown in Figure 1b. SS was chosen as the substrate owing to its cost-effectiveness, excellent hydrophilic and thermal insulating properties, and the unique structure of abundant microchannels.[36] First, CS/CMC is introduced into the SS channels by soaking the SS pieces into the CS/CMC precursor mixture. After the glutaraldehyde was added as the curing agent, the samples are placed in an oven for interaction and then transferred to a freeze-dryer for freeze-drying. Therefore, the open channels in the SS are filled with CS/CMC. Afterward, solar absorber GPs are sprayed on the surface of the SS-CS/CMC to obtain the ultimate SS-CS/CMC-GP device after air-drying. Figure 1c illustrates the formation process of the CS/CMC hydrogel in detail. CS, a

https://doi.org/10.1021/acsami.3c12333
ACS Appl. Mater. Interfaces 2023, 15, 48336−48345

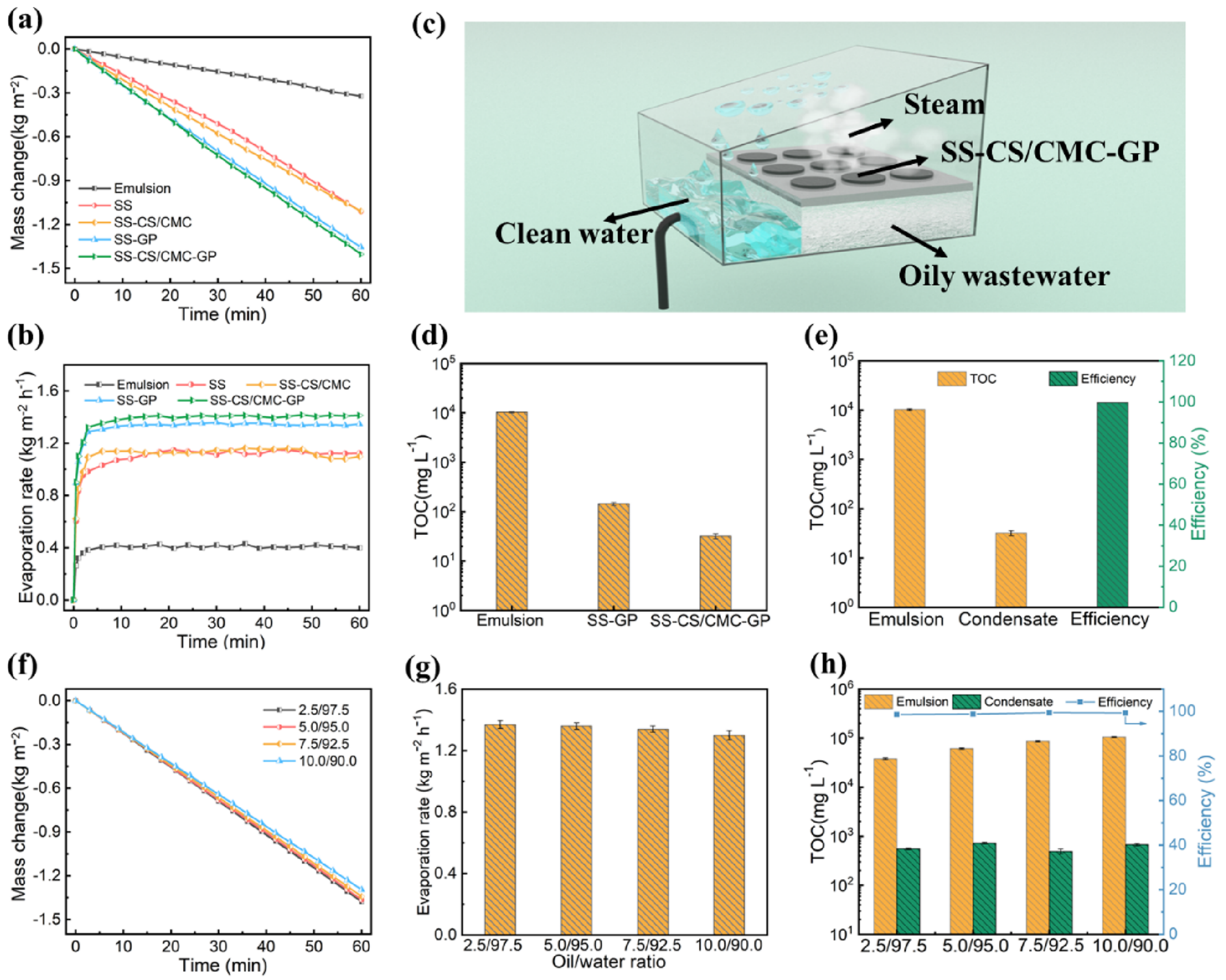

Figure 4. (a) Weight loss and (b) evaporation rates of various evaporators and pure emulsion under 1 sun illumination over time. (c) The evaporation−condensation device diagram of wastewater purification. (d) The TOC contents of soybean oil-in-water emulsion and the obtained water from the SS-GP device and SS-CS/CMC-GP device. (e) The TOC content of the condensate and purification efficiency for soybean oil-in-water emulsion. (f) Mass change and (g) evaporation rate of the SS-CS/CMC-GP device toward emulsions with various oil/water ratios. (h) TOC content and purification efficiency of the condensed water obtained from the different oil/water ratios emulsions.

biopolymer derived from chitin, has abundant reactive functional amino groups and hydroxyl groups, which enable it to interact with anion biopolymers. The inherent richness of adsorption sites in CS has led to its widespread application in the fabrication of membranes for the efficient treatment of various types of contaminations.[41] CMC, a water-soluble derivative of cellulose, is a type of anion biopolymer and has plentiful carboxyl and hydroxyl groups. Because of the positively charged amino groups and negatively charged carboxyl groups, CS can interact with the CMC to form gels under electrostatic attraction.

2.2. Structural Characterization of the Sample. The morphological and microstructural characterizations of the samples are listed in Figure 2. Sugar cane is one of the main farm crops and is widely cultivated in subtropical and tropical areas. Photographs of the sugar cane fruit are shown in Figure 2a. SEM images in Figure 2b,c indicate that the structure of natural SS is composed of vascular bundles and parenchyma cells. The vascular bundles (20−80 μm in diameter) that commonly exist in plants are responsible for water transportation, whereas the honeycomb-like parenchyma cells (100−240 μm in diameter) are well distributed around the vascular bundles for nutrition storage. Figure 2d,e and Figure S1 illustrate that the vascular bundles in the SS were filled with CS/CMC, whereas the original SS channel walls and CS/CMC can be well-recognized. Notably, the microstructure of the SS is well retained after filling with CS/CMC, illustrating its outstanding structure stability. GPs with a thickness of ∼110 μm (Figure S2) are well deposited on the surface of SS-CS/CMC, as evidenced by the SEM image displayed in Figure 2f,g, which facilitate solar absorption and solar−thermal conversion. The corresponding EDS elemental mapping displayed the distribution of elements C, N, and O on the natural SS (Figure 2h and Figure S3). Clearly, element C is most densely distributed on the surface of the SS. The corresponding contents of C, N, and O elements were calculated according to the mapping intensity (Figure S4). The results showed a change in the elemental proportion of the samples. GPs, as one of the carbon materials, were introduced to substantially increase the C content of the device. The C content of SS-CS/CMC-GP (88.01%) was dramatically higher than those of SS (50.03%) and SS-CS/CMC (45.04%). The insets in Figure

https://doi.org/10.1021/acsami.3c12333
ACS Appl. Mater. Interfaces 2023, 15, 48336−48345

2b,d,f are the digital photos of natural SS, SS-CS/CMC, and the SS-CS/CMC-GP device, respectively.

2.3. Wettability and Photothermal Characterization. The surface wettability of the solar-driven evaporator plays a crucial role in water transportation and prevents the infiltration of oil droplets. To investigate the surface wettability, the water contact angle (WCA) of various specimens was measured in the first step. The high surface energy components of plentiful −OH groups in the cellulose of the SS and CS/CMC endowed the SS, SS-CS/CMC, and SS-CS/CMC-GP with superhydrophilic and underwater superoleophobic properties.[42] As displayed in Figure 3a, the WCAs of the various specimens are nearly 0°, indicating thair excellent hydrophilicity. Moreover, the CS/CMC gel fills the pore of the SS, delaying the infiltration of the droplets; thus, the time for droplets to penetrate into the interior of the SS-CS/CMC is longer than that of SS (Figure S5). On the other hand, the underwater oil contact angle (OCA) of the specimen was also measured to evaluate the oleophobic property. Figure 3b shows the OCAs of various oils on the surfaces of SS and SS-CS/CMC. Specifically, the OCAs of soybean oil, silicone oil, and *n*-decane on the SS surface are 152.4 ± 1.2, 153.2 ± 1.6, and 141.7 ± 1.3°, respectively, whereas those on the SS-CS/CMC surface are 156.7 ± 2.2, 157.2 ± 0.9, and 152.7 ± 1.9°, illustrating that the introduction of the CS/CMC gel further improves underwater oleophobicity. This is because the surface of SS-CS/CMC has more −OH groups compared to SS.[42] As shown in Figure S6, it can be seen from the infrared spectrum of the CS/CMC that the wide absorption peak at 3420 cm^{-1} belonged to the stretching vibration of −OH, demonstrating the abundant presence of −OH groups in CS/CMC.

The light absorption capability of the evaporator significantly influences its solar−thermal conversion performance. Figure 3c shows the UV−vis-NIR spectra of the samples. The averaged light absorption (calculated using the solar spectral solar irradiance AM 1.5G) of the SS was 44.1% within the wavelength range 250−2500 nm. Moreover, the SS-CS/CMC shows a higher light absorption of 45.6%, which is mainly attributed to the filling of CS/CMC gel in the SS channels, resulting in a slight decrease in light diffuse reflectance (Figure S7). Moreover, the addition of GPs as superior solar absorber noticeably increased the absorption of the light by the SS-CS/CMC.[43] As the converted heat energy is more concentrated on the surface of the device, the absorption of the SS-CS/CMC-GP evaporator increases to 93.3%, which is conducive to the efficient production of solar vapor.

To evaluate the solar−thermal conversion performance, the surface temperatures of the various specimens were recorded by employing an infrared camera under 1 sun irradiation (Figure S8). As displayed in Figure 3d, the beginning surface temperatures of SS, SS-CS/CMC, and SS-CS/CMC-GP were 23.5, 23.2 and 23.6 °C, respectively, which are adjacent to the room temperature due to the water saturation. The surface temperatures of SS and SS-CS/CMC increased gradually to 27.6 and 27.8 °C after 6 min of solar irradiation and eventually stabilized at 27.7 and 28.3 °C after 10 min of illumination, respectively. By contrast, the surface temperature of the SS-CS/CMC with GP coating reached 31.6 °C rapidly after 6 min of solar illumination and balanced at 33.8 °C after 24 min of solar irradiation. The SS-CS/CMC-GP exhibited excellent solar−thermal conversion performance compared to the SS and SS-CS/CMC, which is consistent with the above trend of the light absorption behavior. However, the temperature change of the pure emulsion before and after 1 h solar irradiation was only 1.6 °C (from 23.6 to 25.2 °C), indicating that the evaporator is beneficial to the water evaporation.

2.4. Solar-Driven Evaporation Performance. To measure the solar-powered evaporation rates of the various devices, the weight loss of the evaporation device was carefully monitored using an electronic balance under constant 1 sun of solar irradiation. A control test with pure oil-in-water emulsion under identical irradiation intensity was also carried out for comparison. As shown in Figure 4a, typical solar-driven evaporation curves of the various evaporators illustrated that the mass loss of the oil-in-water emulsion was approximately linear with the solar illumination time. The corresponding evaporation rates were acquired by calculating the slopes of the weight loss curves. As presented in Figure 4b, the evaporation rates of the samples reach equilibrium after approximately 6−10 min of solar irradiation, coinciding with the time it takes for the surface temperature to stabilize (Figure 3d). Owing to their porous structure, the SS and SS-CS/CMC specimens showed evaporation rates of 1.10 and 1.12 kg m^{-2} h^{-1}, respectively. After decorating with GPs, the evaporation rates of the SS-GP and SS-CS/CMC-GP increase to 1.35 and 1.41 kg m^{-2} h^{-1}, respectively, which are 3.3 and 3.4 times higher than that of pure emulsion (0.41 kg m^{-2} h^{-1}). Compared with SS and SS-CS/CMC, SS-CS/CMC-GP coated with photothermal conversion material GP is capable of absorbing solar energy and converting it into thermal energy, creating a temperature gradient between the material and the surrounding water. This temperature gradient drives the evaporation process. Interestingly, the evaporation rate of the SS-CS/CMC-based evaporator was greater than that of the raw-SS-based one, which verifies the above analysis of light absorption. During the solar-driven process, the evaporator floats in a tank containing oily wastewater with the assistance of foam and is placed inside a distiller plexiglass. Under solar irradiation, the generated steam rises and meets the top plate. Subsequently, the redox mixture condenses and flows into the water collector for further collection, as depicted in Figure 4c. In addition to the investigation of the evaporation performance, the purification capability of device was estimated by measuring the total organic carbon (TOC) content of primary soybean oil-in-water emulsion and the evaporation condensate. The obtained condensed water from the SS-GP evaporator exhibits a high TOC content of 144.3 mg L^{-1}, which was much higher than that of condensed water collected from the SS-CS/CMC-GP evaporator (Figure 4d). As shown in Figure 4e, the TOC values of the primary emulsion and evaporation condensate were 10342.2 and 32.2 mg L^{-1}, respectively, demonstrating a purification efficiency of 99.7%. The above result further verifies that the CS/CMC gel enhances the evaporator performance. In a comprehensive consideration, SS-CS/CMC-GP was selected to carry out the following experiment.

The evaporation and purification properties of the SS-CS/CMC-GP device for emulsions stabilized with various concentrations were also studied. Figure S9a shows the emulsion with different oil/water mass ratios of 2.5/97.5, 5.0/95.0, 7.5/2.5, and 10.0/90.0. With the increases of the oil/water mass ratio, the emulsion becomes more and more milky. It is worth noting that the evaporation rate of the SS-CS/CMC-GP device is not greatly affected by the high oil/water ratio emulsions (Figure 4f). As shown in Figure 4g, the evaporation rates of the SS-CS/CMC-GP evaporator with oil/water mass ratios of 2.5/97.5, 5.0/95.0, 7.5/2.5, and 10.0/90.0

https://doi.org/10.1021/acsami.3c12333
ACS Appl. Mater. Interfaces 2023, 15, 48336−48345

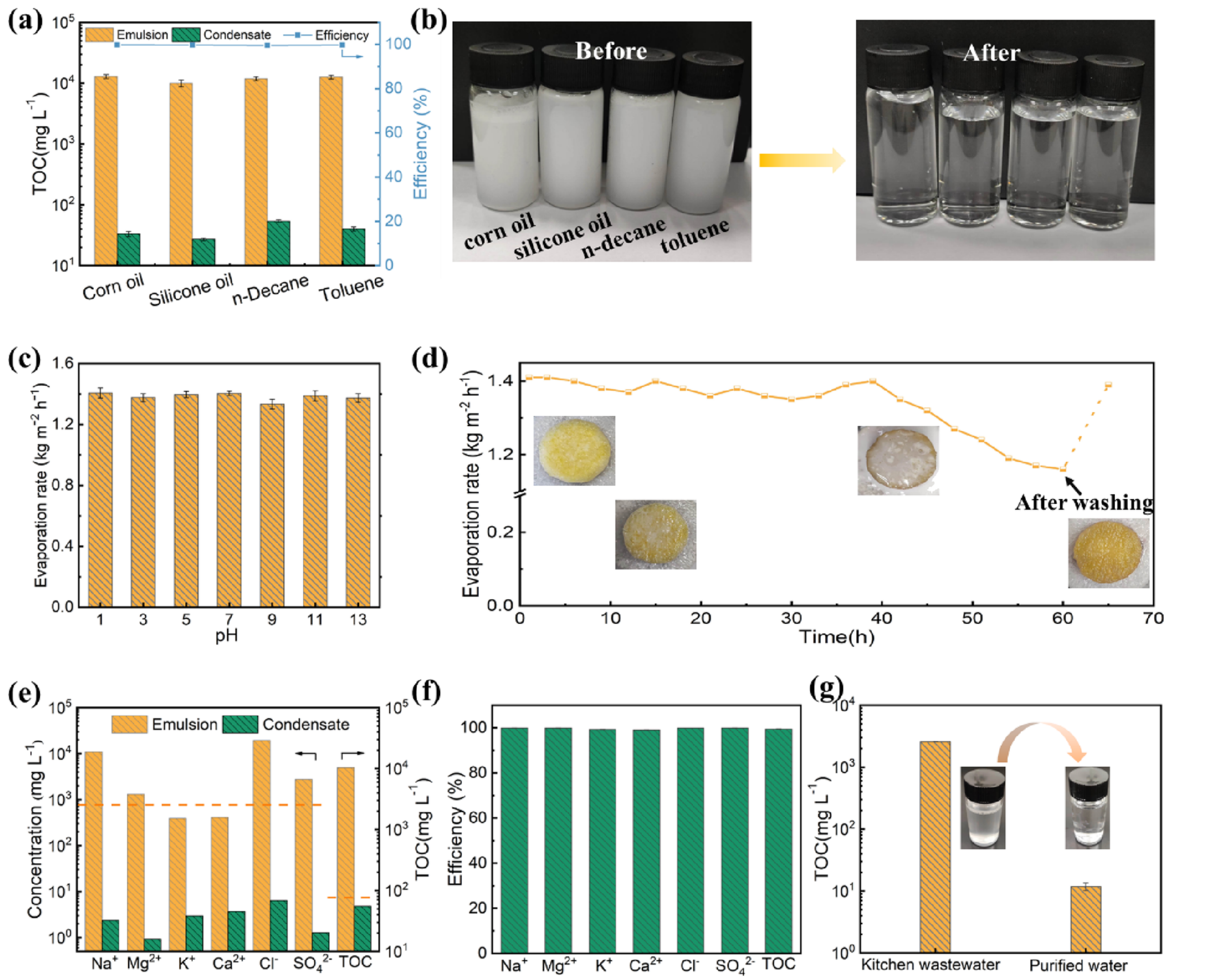

Figure 5. (a) TOC content of different emulsions and the condensate and purification efficiency for different emulsions. (b) Optical photographs of various emulsions before and after purification with the SS-CS/CMC-GP device. (c) The evaporation rates of the soybean oil-in-water emulsion under different pHs. (d) The long-term durability of the SS-CS/CMC-GP device for handing soybean oil-in-water emulsion (insets are the underwater surface of the device under different treating times). (e) Concentrations of six primary ions and the TOC content of the oily seawater before and after the solar-driven desalination and purification. (f) Desalination and purification efficiencies of the oily seawater after the solar-driven treatment. (g) TOC content of the kitchen wastewater before and after solar purification.

were 1.37, 1.36, 1.34, and 1.30 kg m^{-2} h^{-1}, respectively. Figure 4h depicts the purification efficiency of the SS-CS/CMC-GP device for emulsions with different oil concentrations. Specifically, the TOC contents of the above four emulsions were 38049.2, 61219.5, 86146.3, and 104962.6 mg L^{-1}, respectively. After purification by the SS-CS/CMC-GP device, the corresponding collected condensed water displayed low TOC values of 552.4, 726.9, 491.5, and 674.8 mg L^{-1}, respectively. Thus, the calculated purification efficiencies are 98.6, 98.8, 99.4, and 99.3% for 2.5/97.5, 5.0/95.0, 7.5/2.5, and 10.0/90.0 emulsions, respectively. The images in Figure S9b display that clear and transparent clean water was collected from the milky emulsions.

2.5. Solar-Driven Purification and Desalination Performance. To justify the extensive applicability of the solar-powered purification evaporator sufficiently, other surfactant-stabilized emulsions were prepared and tested under 1 sun of solar irradiation. In addition to soybean oil, the purification rates and efficiencies of corn oil-in-water, silicone oil-in-water, *n*-decane-in-water, and toluene-in-water emulsions were also investigated. As shown in Figure S10, more dense oil droplets (<10 μm) are observed in the original emulsions. Interestingly, no droplets are seen in the obtained water after purification treatment. To accurately determine the purification capability of the SS-CS/CMC-GP device, the TOC content of the obtained water from the different emulsions was also measured. As exhibited in Figure 5a, the TOC contents for the original corn oil, silicone oil, *n*-decane, and toluene emulsions were 121916.7, 9965.9, 11840.2, and 12607.4 mg L^{-1}, respectively. After purification by the SS-CS/CMC-GP device, the corresponding condensed water collected from emulsion showed relatively low TOC values of 33.35, 27.13, 53.78, and 40.23 mg L^{-1}, respectively. As a result, the calculated purification efficiencies of corn oil-in-water, silicone oil-in-water, *n*-decane-in-water, and toluene-in-water emulsion are 99.9, 99.7, 99.6, and 99.7%, respectively. All types of emulsions were transformed from a milky liquid to clear and transparent water after treatment (Figure 5b). The high purification efficiency illustrates that the solar-driven SS-CS/CMC-GP evaporator can efficiently remedy various types of

https://doi.org/10.1021/acsami.3c12333
ACS Appl. Mater. Interfaces 2023, 15, 48336−48345

oil-in-water emulsions. Moreover, the evaporation performance of the SS-CS/CMC-GP device for different emulsions was almost the same as that of soybean oil-in-water emulsion (Figure S11). Compared to most previous studies, the purification performance of the SS-CS/CMC-GP device demonstrates superior effectiveness. It is found that the purification efficiency of the SS-CS/CMC-GP device is superior to those of most devices reported previously (Table S1).

Given the complex constituents, oily wastewater puts forward higher requirements for acid and alkali tolerance of the SS-CS/CMC-GP device. Therefore, we determined the evaporation performance of the device and the pH of condensed water obtained from different soybean oil-in-water emulsions with a pH of 1−13. Figure 5c shows that the evaporation rates of the SS-CS/CMC-GP device in emulsions with various pH values ranging from 1 to 13 are 1.41, 1.38, 1.40, 1.40, 1.33, 1.39, and 1.37 kg m^{-2} h^{-1}, respectively, demonstrating that the evaporation rate did not remarkably change compared to the neutral emulsion. The pH test paper of the emulsion before and after purification (Figure S12) reveals that all of the obtained condensed water exhibited a pH of approximately 7 (Figure S13), implying that both acidic and alkaline emulsions were purified effectively, resulting in the generation of clean water. These results suggest that the SS-CS/CMC-GP device is resistant enough for an extensive pH range. Then, the long-term durability of the SS-CS/CMC-GP evaporator was evaluated by recording the evaporation rate for handling soybean emulsions (Figure 5d). The device was placed under continuous 1 sun irradiation. It was found that the evaporation rate of the SS-CS/CMC-GP evaporator could remain stable even after 40 h. As the solar irradiation time increased from 40 to 60 h, the evaporation rate slightly decreased from 1.40 to 1.16 kg m^{-2} h^{-1}. The decrease in the evaporation rate can be attributed to the accumulation of the emulsifier from the emulsion.[20] As displayed in the illustrations in Figure 5d, after purification treatment for 10 h, the milky white emulsifier started to accumulate on the underwater surface and almost covered the entire underwater surface of the SS-CS/CMC-GP evaporator after 40 h. This milky white emulsifier accumulated on the underwater surface of the device can be readily removed by washing with water, confirming that the oil is only adhered to the underwater surface of the evaporator and does not penetrate the inside of the device.[19] As expected, the purification rate of the evaporator returns to its original value. The above results suggest that the SS-CS/CMC-GP evaporator possesses an outstanding long-term durability.

To demonstrate the solar desalination performance of the SS-CS/CMC-GP evaporator, oily seawater was used as the desalination sample. As shown in Figure 5e, after desalination under 1 sun solar illumination, the concentrations of Na^+, Mg^{2+}, K^+, and Ca^{2+} cations and Cl^- and SO_4^{2-} anions and the TOC content of the obtained condensed water were significantly decreased from 10900.91, 1310.63, 391.28, 416.76, 19450.37, 2758.62, and 10342.19 mg L^{-1} to 2.34, 0.93, 2.93, 3.69, 6.37, 1.28, and 55.16 mg L^{-1}, respectively. The purification efficiency of oil and the rejection of cations and anions all exceed 99.9% (Figure 5f). The clean water obtained from the purification process meets the drinking water standards set by the World Health Organization, as indicated by the acceptable levels of the TOC content and ion concentrations (displayed as yellow dashes in Figure 5e). Moreover, the digital photographs of the SS-CS/CMC-GP device after purification for 2 days are also provided in Figure S14. The structural integrity of the device remained intact, without any visible salt accumulation on its surface. Additionally, the concentration of organic compounds in the kitchen wastewater was significantly decreased from 2570.23 to 11.82 mg L^{-1}, demonstrating its excellent purification performance for practical kitchen wastewater (Figure 5g). The above results indicate that the SS-CS/CMC-GP evaporator possesses superior decontamination capability and salt inhibition property for oily seawater purification applications. Moreover, wastewater treatment experiments were further carried out to investigate the wastewater purification capability of the SS-CS/CMC-GP device. Four colorful solutions were chosen to be purified under 1 sun light illumination. As shown in Figure S15a, the main characteristic peaks at 484, 426, 418, and 628 nm are attributed to the absorption peaks of red, yellow, green, and blue dyes, respectively. After solar-powered purification, as shown in Figure S15b, the absorption value of the condensed water is similar to that of distilled water without the characteristic peaks of the dyes shown, indicating that the dye should be effectively removed from the purified water. Figure S16 clearly illustrates the transformation of colored dye water from its initial state to a clear and transparent appearance, underscoring the potential of the SS-CS/CMC-GP evaporator in effectively purifying organic wastewater.

3. CONCLUSIONS

In summary, a plant-inspired solar-driven SS-CS/CMC-GP device was prepared for efficient general-purpose solar-driven oily wastewater purification. The device incorporates a solar-absorbing top layer and a water transportation bottom layer. Because of its unique superhydrophilicity and underwater oleophobicity, abundant microchannels, and excellent solar absorption property, the evaporator demonstrates exceptional effectiveness in oil−water separation and the removal of organic dyes and metal ions from wastewater and seawater. A purification efficiency of 99.9% and an evaporation rate of 1.37−1.41 kg m^{-2} h^{-1} under 1 sun irradiation were achieved by the SS-CS/CMC-GP evaporator, even in an emulsion with high oil/water ratio of 10/90 (g/g). More importantly, the device maintains a stable water evaporation performance and efficient solar purification toward various oil-in-water emulsions. Moreover, the evaporator displayed outstanding acid/alkali resistance and excellent long-term durability. Therefore, this green and renewable biomass-based separator provides a facile strategy for purifying oily wastewater and producing clean water from oily wastewater or seawater.

4. EXPERIMENTAL SECTION

4.1. Materials. Fresh sugar canes were purchased from Guangxi Region, China. Soybean oil and corn oil were obtained from the Taobao store. Silicone oil, toluene, Tween 80, acetic acid, sodium dodecyl sulfate (SDS), GP, and CS with degree of deacetylation of 90.0% and viscosity-average molecular weight of 62 kDa were supplied by Sinopharm Chemical Reagent Co., Ltd. (China). Glutaraldehyde (50% water solution), *n*-decane, and CMC with a degree of substitution of 1.0 were bought from Shanghai Macklin Biochemical Co., Ltd. (China). All chemical reagents were used without further purification.

4.2. Preparation of SS-CS/CMC-GP and SS-GP Devices. The samples used in this work were extracted from the stem part of sugar cane. Briefly, the skinned sugar cane was cut into cylindrical pieces (diameter: 2.0 cm, height: 2.0 cm) along the growth direction, boiled in water, and dried to obtain sugar cane stem (SS) specimen. Meanwhile, CS solution (1 wt %) and CMC solution (1 wt %) were mixed evenly by stirring to prepare the precursor solution of CS/CMC hydrogels. Then, the SS samples were immersed in precursor solutions for 12 h. And then, 300 μL of glutaraldehyde liquid was introduced into 40 mL of the aforementioned mixture and stirred in an ice bath for 10 min. Next, all of the samples were maintained at 60 °C to react for 3 h. Finally, samples were rinsed with deionized water to remove the unreacted reagents and freeze-dried in a freeze-dryer for 48 h, and the SS-CS/CMC was prepared.

GP was carefully mixed with deionized water to prepare a GP dispersion (10 mg mL^{-1}). Afterward, the well-dispersed solution was sprayed evenly on the surface of SS-CS/CMC. After being dried in air, the SS-CS/CMC-GP evaporator was obtained. As a control sample, the GP dispersion was spread evenly onto the surface of SS to acquire the SS-GP evaporator.

4.3. Preparation of Oil-in-Water Emulsions. Soybean oil (1.0 g), Tween 80 (0.1 g), and water (99.0 g) were mixed and sheared at high speed (8000 rpm) for 15 min to prepare a soybean oil-in-water emulsion. The preparations of corn oil-in-water emulsion and silicone oil-in-water emulsion were handled the same as those of soybean oil-in-water emulsion. Soybean emulsions with different oil/water ratios of 2.5/97.5, 5.0/95.0, 7.5/92.5, and 10.0/90.0 were also prepared according to the same oil/Tween 80 ratio, respectively. Similarly, *n*-decane (1 g)/toluene (1 g), SDS (0.5 g), and water (99 g) were mixed and subjected to shearing to obtain an *n*-decane-in-water emulsion and toluene-in-water emulsion. The oily seawater was obtained by dissolving 3.5% bay salt in a soybean oil-in-water emulsion.

4.4. Characterization. The morphology and element mapping of the samples were investigated by using field-emission scanning electron microscopy (Tescan MAIA3 XMH, 10 kV). The water and underwater oil contact angles were determined with a LAUDA Scientific GmbH, LSA-100 instrument. The optical properties, including transmittance (T) and reflectance (R) spectra within the 200−2500 nm range, were captured by using a UV-3600 spectrometer fitted with an integrating sphere. The absorption (A) values were calculated by $A = 1 - R - T$. Fourier transform infrared (FT-IR) spectra were obtained by a Nicolet iS10 FTIR spectrometer. The concentration of major metal ions in both predesalination and postdesalination water was evaluated using inductively coupled plasma optical emission spectroscopy (Agilent 720ES). The concentrations of chloride ions (Cl^-) and sulfate ions (SO_4^{2-}) before and after desalination were measured using an ion chromatograph instrument (ICS-1100). The optical absorption spectra of the dye solutions and collected clean water were recorded by using a UV−vis spectrometer (UV-3600, Shimadzu). The TOC values of the emulsions and condensates were quantified by employing a TOC analyzer (Vario TOC).

4.5. Oily Wastewater Purification Experiment. The solar-driven purification experiment was conducted by employing a conventional solar simulator (PLS-SXE300UV) as the illumination source. The irradiation intensity was calibrated by using a light intensity meter. A calibrated electronic balance with a precision of 0.1 mg was utilized to monitor the changes in the mass of the oily water. The experiments related to water evaporation were performed under ambient conditions at around 25 °C accompanied by a relative humidity of approximately 60%. Monitoring the upper surface temperature of the sample was accomplished by using a thermal infrared camera (FLUKE-VT04).

■ ASSOCIATED CONTENT

Supporting Information

The Supporting Information is available free of charge at https://pubs.acs.org/doi/10.1021/acsami.3c12333.

Microstructure of SS and SS-CS/CMC; the side-view SEM image of SS-CS/CMC-GP; the EDS spectrum, surface wettability, and reflectance spectra of SS, SS-CS/CMC, and SS-CS/CMC-GP; infrared images of SS-CS/CMC and SS-CS/CMC-GP immersed in emulsion under 1 sun illumination at various time points; the TOC contents of soybean oil-in-water emulsion and the obtained water from the SS-GP device and SS-CS/CMC-GP device; digital photos of the soybean oil-in-water emulsions with different oil/water ratios before and after purification; optical images of various emulsions before and after purification; mass change and evaporation rate of four different emulsions under 1 sun irradiation; and optical photograph of the SS-CS/CMC-GP device for purifying soybean oil-in-seawater (PDF)

■ AUTHOR INFORMATION

Corresponding Authors

Jianfeng Shen − *Institute of Special Materials and Technology, Fudan University, Shanghai 200433, P.R. China;* orcid.org/0000-0002-8835-6292; Email: jfshen@fudan.edu.cn

Mingxin Ye − *Institute of Special Materials and Technology, Fudan University, Shanghai 200433, P.R. China;* orcid.org/0000-0002-4532-2594; Email: mxye@fudan.edu.cn

Authors

Zhenglong Xu − *Institute of Special Materials and Technology and Department of Materials Science, Fudan University, Shanghai 200433, P.R. China*

Yifan Yang − *Institute of Special Materials and Technology and Department of Materials Science, Fudan University, Shanghai 200433, P.R. China*

Wei Yao − *Institute of Special Materials and Technology and Department of Materials Science, Fudan University, Shanghai 200433, P.R. China*

Chuming Ye − *Institute of Special Materials and Technology and Department of Materials Science, Fudan University, Shanghai 200433, P.R. China*

Haohui Qiao − *Institute of Special Materials and Technology and Department of Materials Science, Fudan University, Shanghai 200433, P.R. China*

Complete contact information is available at: https://pubs.acs.org/10.1021/acsami.3c12333

Author Contributions

Z.X. designed the research, performed most of the experiments, and wrote the paper; Y.Y. analyzed the data; W.Y. measured the contact angle of the sample; C.Y. and H.Q. discussed the results; J.S. and M.Y. supervised all research phases. All authors have given approval to the final version of the manuscript.

Notes

The authors declare no competing financial interest.

■ ACKNOWLEDGMENTS

The authors gratefully acknowledge the financial support from the National Natural Science Foundation of China (51972064, 52222315).

■ REFERENCES

(1) Han, L.; Shen, L.; Lin, H.; Cheng, T.; Wen, J.; Zeng, Q.; Xu, Y.; Li, R.; Zhang, M.; Hong, H.; Tang, C.; Wang, Z. L. Three Dimension-

https://doi.org/10.1021/acsami.3c12333
ACS Appl. Mater. Interfaces 2023, 15, 48336−48345

Printed Membrane for Ultrafast Oil/Water Separation as Driven by Gravitation. *Nano Energy* **2023**, *111*, 10835.
(2) Zhu, R.; Wang, D.; Liu, Y.; Liu, M.; Fu, S. Bifunctional Superwetting Carbon Nanotubes/Cellulose Composite Membrane for Solar Desalination and Oily Seawater Purification. *Chem. Eng. J.* **2022**, *433*, No. 133510.
(3) Zhang, J.; Liu, L.; Si, Y.; Yu, J.; Ding, B. Electrospun Nanofibrous Membranes: An Effective Arsenal for the Purification of Emulsified Oily Wastewater. *Adv. Funct. Mater.* **2020**, *30*, 2002191.
(4) Ying, T.; Su, J.; Jiang, Y.; Ni, L.; Jiang, X.; Ke, Q.; Xu, H. Superhydrophobic Mofs Decorated on Hierarchically Micro/Nanofibrous Membranes for High-Performance Emulsified Oily Wastewater Separation and Cationic Dyes Adsorption. *J. Mater. Chem. A* **2022**, *10*, 829−845.
(5) Wang, F. P.; Zhao, X. J.; Wahid, F.; Zhao, X. Q.; Qin, X. T.; Bai, H.; Xie, Y. Y. C.; Zhong, C.; Jia, S. R. Sustainable, Superhydrophobic Membranes Based on Bacterial Cellulose for Gravity-Driven Oil/Water Separation. *Carbohydr. Polym.* **2021**, *253*, No. 117220.
(6) Wang, Y.; Zhou, L.; Luo, X.; Zhang, Y.; Sun, J.; Ning, X.; Yuan, Y. Solar-Heated Graphene Sponge for High-Efficiency Clean-up of Viscous Crude Oil Spill. *J. Clean. Prod.* **2019**, *230*, 995−1002.
(7) Mirshafiee, A.; Rezaee, A.; Mamoory, R. S. A Clean Production Process for Edible Oil Removal from Wastewater Using an Electroflotation with Horizontal Arrangement of Mesh Electrodes. *J. Clean. Prod.* **2018**, *198*, 71−79.
(8) Bao, Z.; Chen, D.; Li, N.; Xu, Q.; Li, H.; He, J.; Lu, J. Superamphiphilic and Underwater Superoleophobic Membrane for Oil/Water Emulsion Separation and Organic Dye Degradation. *J. Membr. Sci.* **2020**, *598*, No. 117804.
(9) Zhu, Y.; Wang, J.; Zhang, F.; Gao, S.; Wang, A.; Fang, W.; Jin, J. Zwitterionic Nanohydrogel Grafted Pvdf Membranes with Comprehensive Antifouling Property and Superior Cycle Stability for Oil-in-Water Emulsion Separation. *Adv. Funct. Mater.* **2018**, *28*, 1804121.
(10) Wang, Y.; Yang, S.; Zhang, J.; Chen, Z.; Zhu, B.; Li, J.; Liang, S.; Bai, Y.; Xu, J.; Rao, D.; Dong, L.; Zhang, C.; Yang, X. Scalable and Switchable Co(2)-Responsive Membranes with High Wettability for Separation of Various Oil/Water Systems. *Nat. Commun.* **2023**, *14*, 1108.
(11) Ding, Y.; Wang, J.; Wu, J.; Wang, J.; Liu, F. Binary Nanofibrous Membranes with Independent Oil/Water Transport Channels for Durable Emulsion Separation. *J. Membr. Sci.* **2023**, *673*, No. 121484.
(12) Long, Q.; Chen, J.; Wang, Z.; Zhang, Z.; Qi, G.; Liu, Z.-Q. Vein-supported Porous Membranes with Enhanced Superhydrophilicity and Mechanical Strength for Oil-water Separation. *Sep. Purif. Technol.* **2021**, *254*, No. 117517.
(13) Long, Q.; Zhao, S.; Chen, J.; Zhang, Z.; Qi, G.; Liu, Z.-Q. Self-assembly Enabled Nano-intercalation for Stable High-performance MXene Membranes. *J. Membr. Sci.* **2021**, *635*, No. 119464.
(14) Sun, Q.; Du, J.; Wang, L.; Yao, A.; Song, Z.; Liu, L.; Cao, D.; Ma, J.; Lim, W.; He, W.; Ul Hassan, S.; Zhou, C.; Liu, J. Smart Superwetting Cof Membrane for Controllable Oil/Water Separation. *Sep. Purif. Technol.* **2023**, *317*, No. 123825.
(15) Chai, J.; Wang, G.; Zhang, A.; Li, X.; Xu, Z.; Zhao, J.; Zhao, G. Robust Polytetrafluoroethylene (Ptfe) Nanofibrous Membrane Achieved by Shear-Induced in-Situ Fibrillation for Fast Oil/Water Separation and Solid Removal in Harsh Solvents. *Chem. Eng. J.* **2023**, *461*, No. 141971.
(16) Zhang, Y.; Zhang, G.; Li, B.; Wu, L. Non-Stop Switching Separation of Superfine Solid/Liquid Dispersed Phases in Oil and Water Systems Using Polymer-Assisted Framework Fiber Membranes. *Small Methods* **2023**, *7*, 2201455.
(17) Li, H.; Zhang, J.; Gan, S.; Liu, X.; Zhu, L.; Xia, F.; Luo, X.; Xue, Q. Bioinspired Dynamic Antifouling of Oil-Water Separation Membrane by Bubble-Mediated Shape Morphing. *Adv. Funct. Mater.* **2023**, *33*, 2212582.
(18) Oh, S.; Bang, J.; Jin, H.-J.; Kwak, H. W. Green Fabrication of Underwater Superoleophobic Biopolymeric Nanofibrous Membranes for Effective Oil−Water Separation. *Adv. Fiber Mater.* **2023**, *5*, 603−616.
(19) Yao, W.; Tan, J.; Zhu, X.; Liu, G.; Xu, Z.; Ye, M.; Shen, J. Leaf-Structure-Inspired Photothermal Evaporator for Versatile Oily Wastewater Purification. *Cell Rep. Phys. Sci.* **2022**, *3*, No. 101020.
(20) Wang, Z.; Guo, P.; Heng, L.; Jiang, L. Nano/Submicrometer-Emulsion Oily Wastewater Treatment Inspired by Plant Transpiration. *Matter* **2021**, *4*, 1274−1286.
(21) Liu, X.; Hou, G.; Zhao, J.; Zhao, W.; Xu, Q.; Zheng, X.; Liu, Z.; Lai, Y. Self-Interlocked Down Biomass-Based Carbon Fiber Aerogel for Highly Efficient and Stable Solar Steam Generation. *Chem. Eng. J.* **2023**, *465*, No. 142826.
(22) Fu, J.; Li, Z.; Li, X.; Sun, F.; Li, L.; Li, H.; Zhao, J.; Ma, J. Hierarchical Porous Metallic Glass with Strong Broadband Absorption and Photothermal Conversion Performance for Solar Steam Generation. *Nano Energy* **2023**, *106*, No. 108019.
(23) Lin, X.; Wang, P.; Hong, R.; Zhu, X.; Liu, Y.; Pan, X.; Qiu, X.; Qin, Y. Fully Lignocellulosic Biomass-Based Double-Layered Porous Hydrogel for Efficient Solar Steam Generation. *Adv. Funct. Mater.* **2022**, *32*, 2209262.
(24) Peng, B.; Lyu, Q.; Li, M.; Du, S.; Zhu, J.; Zhang, L. Phase-Separated Polyzwitterionic Hydrogels with Tunable Sponge-Like Structures for Stable Solar Steam Generation. *Adv. Funct. Mater.* **2023**, *33*, 2214045.
(25) Yu, B.; Wang, Y.; Zhang, Y.; Zhang, Z. Self-Supporting Nanoporous Copper Film with High Porosity and Broadband Light Absorption for Efficient Solar Steam Generation. *Nano-Micro Lett.* **2023**, *15*, 94.
(26) Hu, Y.; Ma, H.; Wu, M.; Lin, T.; Yao, H.; Liu, F.; Cheng, H.; Qu, L. A Reconfigurable and Magnetically Responsive Assembly for Dynamic Solar Steam Generation. *Nat. Commun.* **2022**, *13*, 4335.
(27) Torres, J. F.; Tsuda, K.; Murakami, Y.; Guo, Y.; Hosseini, S.; Asselineau, C.-A.; Taheri, M.; Drewes, K.; Tricoli, A.; Lipiński, W.; Coventry, J. Highly Efficient and Durable Solar Thermal Energy Harvesting Via Scalable Hierarchical Coatings Inspired by Stony Corals. *Energy Environ. Sci.* **2022**, *15*, 1893−1906.
(28) Zhu, M.; Li, Y.; Chen, F.; Zhu, X.; Dai, J.; Li, Y.; Yang, Z.; Yan, X.; Song, J.; Wang, Y.; Hitz, E.; Luo, W.; Lu, M.; Yang, B.; Hu, L. Plasmonic Wood for High-Efficiency Solar Steam Generation. *Adv. Energy Mater.* **2018**, *8*, 1701028.
(29) Sun, Z.; Wang, J.; Wu, Q.; Wang, Z.; Wang, Z.; Sun, J.; Liu, C. J. Plasmon Based Double-Layer Hydrogel Device for a Highly Efficient Solar Vapor Generation. *Adv. Funct. Mater.* **2019**, *29*, 1901312.
(30) Guan, W.; Guo, Y.; Yu, G. Carbon Materials for Solar Water Evaporation and Desalination. *Small* **2021**, *17*, 2007176.
(31) Cao, P.; Zhao, L.; Zhang, J.; Zhang, L.; Yuan, P.; Zhang, Y.; Li, Q. Gradient Heating Effect Modulated by Hydrophobic/Hydrophilic Carbon Nanotube Network Structures for Ultrafast Solar Steam Generation. *ACS Appl. Mater. Interfaces* **2021**, *13*, 19109−19116.
(32) Zhang, P.; Zhao, F.; Shi, W.; Lu, H.; Zhou, X.; Guo, Y.; Yu, G. Super Water-Extracting Gels for Solar-Powered Volatile Organic Compounds Management in the Hydrological Cycle. *Adv. Mater.* **2022**, *34*, 2110548.
(33) Yang, P.; Bai, W.; Zou, Y.; Zhang, X.; Yang, Y.; Duan, G.; Wu, J.; Xu, Y.; Li, Y. A Melanin-Inspired Robust Aerogel for Multifunctional Water Remediation. *Mater. Horiz.* **2023**, *10*, 1020−1029.
(34) Chen, L.; Mu, X.; Guo, Y.; Lu, H.; Yang, Y.; Xiao, C.; Hasi, Q. Mxene-Doped Kapok Fiber Aerogels with Oleophobicity for Efficient Interfacial Solar Steam Generation. *J. Colloid Interface Sci.* **2022**, *626*, 35−46.
(35) Brunner, I.; Herzog, C.; Dawes, M. A.; Arend, M.; Sperisen, C. How Tree Roots Respond to Drought. *Front. Plant Sci.* **2015**, *6*, 547.
(36) Liu, J.; Liu, Q.; Ma, D.; Yuan, Y.; Yao, J.; Zhang, W.; Su, H.; Su, Y.; Gu, J.; Zhang, D. Simultaneously Achieving Thermal Insulation and Rapid Water Transport in Sugarcane Stems for Efficient Solar Steam Generation. *J. Mater. Chem. A* **2019**, *7*, 9034−9039.
(37) Wheeler, T. D.; Stroock, A. D. The Transpiration of Water at Negative Pressures in a Synthetic Tree. *Nature* **2008**, *455*, 208−212.
(38) Pieruschka, R.; Huber, G.; Berry, J. A. Control of Transpiration by Radiation. *Proc. Natl. Acad. Sci. U.S.A.* **2010**, *107*, 13372−13377.

(39) Zhuang, S.; Zhou, L.; Xu, W.; Xu, N.; Hu, X.; Li, X.; Lv, G.; Zheng, Q.; Zhu, S.; Wang, Z.; Zhu, J. Tuning Transpiration by Interfacial Solar Absorber-Leaf Engineering. *Adv. Sci.* **2018**, *5*, 1700497.

(40) Gong, F.; Wang, W.; Li, H.; Xia, D.; Dai, Q.; Wu, X.; Wang, M.; Li, J.; Papavassiliou, D. V.; Xiao, R. Solid Waste and Graphite Derived Solar Steam Generator for Highly-Efficient and Cost-Effective Water Purification. *Appl. Energy* **2020**, *261*, No. 114410.

(41) Long, Q.; Zhang, Z.; Qi, G.; Wang, Z.; Chen, Y.; Liu, Z.-Q. Fabrication of Chitosan Nanofiltration Membranes by the Film Casting Strategy for Effective Removal of Dyes/Salts in Textile Wastewater. *ACS Sustainable Chem. Eng.* **2020**, *8*, 2512−2522.

(42) Lv, W.; Mei, Q.; Xiao, J.; Du, M.; Zheng, Q. 3d Multiscale Superhydrophilic Sponges with Delicately Designed Pore Size for Ultrafast Oil/Water Separation. *Adv. Funct. Mater.* **2017**, *27*, 1704293.

(43) Panchal, H.; Sadasivuni, K. K.; Ahmed, A. A. A.; Hishan, S. S.; Doranehgard, M. H.; Essa, F. A.; Shanmugan, S.; Khalid, M. Graphite Powder Mixed with Black Paint on the Absorber Plate of the Solar Still to Enhance Yield: An Experimental Investigation. *Desalination* **2021**, *520*, No. 115349.

https://doi.org/10.1021/acsami.3c12333
ACS Appl. Mater. Interfaces 2023, 15, 48336−48345